Attribution of observed changes in extreme temperatures to anthropogenic forcing using CMIP6 models

Weather and Climate Extremes 39 (2023) 100548

Contents lists available at ScienceDirect

Weather and Climate Extremes

journal homepage: www.elsevier.com/locate/wace

Attribution of observed changes in extreme temperatures to anthropogenic forcing using CMIP6 models

Mastawesha Misganaw Engdaw [a,b,*], Andrea K. Steiner [a,b], Gabriele C. Hegerl [c], Andrew P. Ballinger [c]

[a] Wegener Center for Climate and Global Change, University of Graz, Graz, Austria
[b] FWF-DK, Climate Change, University of Graz, Graz, Austria
[c] School of Geosciences, University of Edinburgh, Edinburgh, United Kingdom

ARTICLE INFO

Keywords:
Climate change
Temperature extremes
Detection
Attribution
CMIP6

ABSTRACT

Global warming has clearly affected the occurrence of extreme events in recent years. Here, we assess changes in the frequency of temperature extremes and their causes, using percentile-based indices. Cold extremes are defined as temperatures below the 10th percentile of daily minimum (TN10) and maximum (TX10) temperatures while hot extremes exceed the 90th percentile of daily minimum (TN90) and maximum (TX90) temperatures. We analyze Berkeley Earth Surface Temperature (BEST) for observed changes in the last four decades 1981-2020, for two extended seasons, boreal summer April–September (AMJJAS) and boreal winter October–March (ONDJFM), and evaluate results using several reanalysis data sets. For the attribution of causes we use CMIP6 climate model simulations, analyzing natural-only and anthropogenic-only forcings. We use an attribution method that accounts for climate modeling uncertainty in both amplitude and pattern of responses.

The observations show detectable changes in both cold and hot extreme temperatures. Hot extremes have increased in all regions and in both seasons while cold extremes have decreased over the past decades. Our attribution analysis revealed anthropogenic forcings are robustly detectable and the main drivers of observed changes in all indices for all regions, consistently in all data sets. Contributions from natural forcings are found small and detectable only in a few regions mainly for daytime cold extremes in ONDJFM. Anthropogenic forcing contributed to an increase of 3.4 days per decade in TN90 and of 2.7 days per decade in TX90, on average, at the global scale. Regionally, the anthropogenic contribution caused a range of decrease of 2–4.7 days per decade in TN10, 1.5–3.6 days per decade in TX10 while it caused an increase of 2.2–4.8 days per decade for TN90 and 2–3.3 days per decade in TX90. Anthropogenic-only warming in ONDJFM is slightly less than in AMJJAS.

1. Introduction

Human influence on the climate system is a well-established fact, and is unequivocally the primary cause of increasing global warming (IPCC, 2014, 2021). In addition to human-induced changes to the mean climate state, climate extremes have also been changing in terms of magnitude or frequency with large impacts on humans and ecosystems (Seneviratne et al., 2021).

Attribution science determines the causes of detected changes. The Intergovernmental Panel on Climate Change (IPCC) defines attribution as "the process of evaluating the relative contributions of multiple causal factors to an observed change in climate variables (e.g., global surface temperature, global mean sea level change), or to the occurrence of extreme weather or climate-related events" (IPCC, 2021). The attribution of change in climate extremes assesses to what extent human-induced climate change has contributed to the magnitude or occurrence probability of extreme events and associated impacts (Stott et al., 2016). Attribution studies can provide input to inform climate change adaptation and mitigation measures as well as quantitative estimates for climate litigation (Allen, 2003; Stott et al., 2016). These studies can also help the public understand whether, and to what extent, changes in climate extremes are caused by human activity (Jézéquel et al., 2020).

Anthropogenic forcing has been attributed as the main driver of the observed increase in global mean temperature with an extremely high level of confidence (Hegerl et al., 1996, 1997, 2019; Gillett et al., 2021).

* Corresponding author. Wegener Center for Climate and Global Change, University of Graz, Graz, Austria.
E-mail addresses: mastawesha.engdaw@uni-graz.at, mastaweshamisganaw@gmail.com (M.M. Engdaw).

https://doi.org/10.1016/j.wace.2023.100548
Received 15 August 2022; Received in revised form 2 January 2023; Accepted 3 January 2023
Available online 4 January 2023

The IPCC's recent Sixth Assessment Report (AR6) states "The likely range of human-induced warming in global-mean surface air temperature (GSAT) in 2010–2019 relative to 1850–1900 is 0.8°C–1.3 °C, encompassing the observed warming of 0.9°C–1.2 °C, while the change attributable to natural forcings is only −0.1 °C to 0.1 °C" (IPCC, 2021). In addition, extreme temperatures and warm spells have shown significant change in probability, magnitude, or duration in almost all regions of the world (Perkins-Kirkpatrick and Lewis, 2020). Different metrics indicate significant changes in cold and hot temperature extremes in different parts of the world at different spatiotemporal scales (Morak et al., 2011; Cowan et al., 2014; Christidis et al., 2015; Fischer and Knutti, 2015; Alexander, 2016; Dong et al., 2017, 2018; Li et al., 2018; Yin et al., 2019; Engdaw et al., 2021; Tan et al., 2021). Anthropogenic forcing is the main contributor to changes in mean temperature (Hegerl et al., 2019; Gillett et al., 2021), its seasonality (Duan et al., 2019) and extreme temperatures (Fischer and Knutti, 2015; Stott et al., 2016; Dittus et al., 2016; Li et al., 2018; Dong et al., 2018; Yin et al., 2019; Christidis et al., 2020). The contribution of anthropogenic forcing is quasi-linearly increasing with time, as the atmospheric concentration of greenhouse gases increases due to emissions from fossil fuels.

Climate model simulations of the sixth Coupled Model Intercomparison Project (CMIP6, Eyring et al., 2016) have recently been made available for analysing past climate and future projections. Improvements in CMIP6 climate models include higher spatial resolution, improved parameterizations (e.g., clouds), and integration of additional Earth system processes and components such as improved sea ice models, and inclusion of nutrient limitations in the terrestrial carbon cycle (Eyring et al., 2016). However, the improvement in performance is less clear, and there is a wider range of equilibrium climate sensitivity (Zelinka et al., 2020). The IPCC AR6 states with very high confidence that "The CMIP6 model ensemble reproduces the observed historical global surface temperature trend and variability with biases small enough to support detection and attribution of human-induced warming". Besides the improved developments of CMIP6 climate models from their predecessors, temperature is among those variables for which the models show the highest pattern correlation with observations (Eyring et al., 2021). CMIP6 climate models realistically represent temperature extremes and reliably reproduce statistics of extremes in observations (IPCC, 2021; van Oldenborgh et al., 2021). The performance of CMIP6 models in simulating extreme temperatures has been evaluated in recent studies: for different regions globally (Chen et al., 2020; Kim et al., 2020; Li et al., 2020; Wu et al., 2021, IPCC, 2021), and for continents including Australia (Deng et al., 2021), Northern America and Europe (Thorarinsdottir et al., 2020; Masud et al., 2021), and Southern America (Almazroui et al., 2021). These studies indicate that CMIP6 models simulate extreme temperatures reasonably well, with modest improvement over their predecessors (CMIP5), although the improvements vary depending on the aspect of interest (spatial patterns, temporal scales, and indices). Comparative studies of model performance have shown that the spread in performance among models is much smaller in CMIP6 than CMIP5 (Chen et al., 2020). CMIP6 models are performing quite well in reproducing the magnitudes and spatial patterns of hot temperature extremes and particularly of cold extremes (IPCC, 2021), which may have been underestimated by the CMIP5 models in previous studies (Yin et al., 2019). CMIP6 models are performing quite well in reproducing the magnitudes and spatial patterns of hot temperature extremes and particularly of cold extremes (IPCC, 2021). This might be due to better representation of underlying processes in CMIP6 such as seasonal and diurnal variability, and synoptic-scale variability (Di Luca et al., 2020; IPCC, 2021). Furthermore, the CMIP6 models simulate the temporal evolution of extreme temperatures well (Wu et al., 2021). In addition to improvements in reproducing multiple aspects of temperature extremes in CMIP6 models, also the representation of natural forcing has improved which is an essential prerequisite for reproducible and reliable attribution statements. The development in the CMIP6 generation of climate models benefits the detection and attribution of temperature extremes. Considering these improvements, CMIP6 climate models are used to attribute changes in intensity of temperature extremes (Gillett et al., 2021, IPCC, 2021).

In this study, we analyze and attribute changes in the frequency of temperature extremes using CMIP6 simulations. We use gridded observational and reanalysis data, as this allows to calculate indices for the frequency of extremes from grid point values, which renders results more comparable to climate model data, while gridded indices of extremes first calculate station-based indices and then are gridded (e.g., Dunn et al., 2020). We then attribute the causes of observed changes to a combination of natural and anthropogenic forcings. We apply a recent detection and attribution method that accounts for uncertainty in pattern and amplitude of the forced response to evaluate the cause of changes in the frequency of temperature extremes at global and regional scales. Thus, in this paper we focus on changes in the frequency of temperature extremes, using observational data and reanalyses, and relying on new CMIP6 simulations. We focus on the past four decades, a period of strong warming, as reanalysis data are more homogeneous over the satellite era. Our results provide compelling evidence that most of the significant changes in the frequency of hot and cold days are due to anthropogenic forcing, with a detectable additional contribution by natural forcing in cold extremes in some regions, largely due to the recovery from the Mount Pinatubo eruption.

2. Data and methods

2.1. Observational and model data

The Berkeley Earth Surface Temperature (BEST) is the observational data set used in this study and available at http://berkeleyearth.org/ (Rohde et al., 2013b). BEST uses all globally available daily recorded station data from 14 databases of the major temperature data reconstruction groups, including the Climatic Research Unit of the University of East Anglia (CRU), the National Aeronautics and Space Administration Goddard Institute for Space Studies (NASA GISS), and the National Oceanic and Atmospheric Administration (NOAA) (Rohde et al., 2013a). Station data are interpolated to 1^{o} X 1^{o} grid resolution using a Kriging interpolation technique as the station coverage varies with time and regions. The spatial coverage has increased to 95% and to 99.9% of Earth's surface in 1960 and 2015, respectively (Rohde and Hausfather, 2020). Although the BEST data set has a good coverage for most of the Earth's surface in the analysis period (1981-2020), we note the influence of data sparseness on the results, which is addressed by kriging, e.g., interpolation with neighbouring stations. Antarctica is the region where BEST data coverage is most scarce (IPCC, 2021).

Some detection and attribution studies of changes in (temperature) extremes (for example, Hu et al., 2020; Seong et al., 2021) used different versions of the Hadley Center's HadEX observational data set (Alexander et al., 2006; Donat et al., 2013; Dunn et al., 2020, https://www.metoffice.gov.uk/hadobs/hadex3/). Extreme indices in HadEX are computed at point-level from station data that are then gridded using an angular-distance weighting method. In this study, we compute indices at grid level using daily gridded observations which enables direct comparison of change in the frequency of extremes between grid point based indices from BEST, reanalysis data and models (Dunn et al., 2020).

However, for further comparison with BEST, we also used HadEX3 data for selected regions where station data are densely available.

We assess the robustness of results from the BEST data set by alternatively using three state-of-the-art reanalysis data sets; National Oceanic Atmospheric Administration's 20 century reanalysis version 3 (20C; Slivinski et al., 2021; https://psl.noaa.gov/data/20thC_Rean/), the European Centre for Medium-Range Weather Forecasts Reanalysis 5 (ERA5; Hersbach et al., 2020, https://cds.climate.copernicus.eu/cdsapp#!/home), and the Japanese Meteorological Agency's 55-year reanalysis (JRA55; Kobayashi et al., 2015, https://jra.kishou.go.jp/JRA-55/index_en.html), as reanalyses infill data gaps

dynamically, while BEST does so statistically. The 20C, ERA5 and JRA55 data sets have 1° X 1°, 0.25° X 0.25° and 1.25° X 1.25° grid resolutions, respectively. The 20C reanalysis is available until 2015 while all the other data sets are available until 2020, hence 20C is here only used for evaluation of the other, longer datasets. Trends in reanalysis data sets are potentially affected by changes in the data stream, which is more consistent with time for 20C and ERA reanalyses than JRA55. Uncertainties are different between these data sets and hence we consider their combined use as a suitable robustness test.

The robustness of BEST and reanalyses data sets is higher since the 1980s because the global observing system improved substantially and more observations became available with better coverage in time and space for most geographic regions (including known data-scarce regions), and also satellite data being assimilated in reanalyses (e.g., Hersbach et al., 2020; Kobayashi et al., 2015; Rohde et al., 2013). Therefore, we use the period 1981-2020 based on more homogenous data sets for our attribution study, which can be conducted for all geographic regions over land. The chosen analysis period enables, when compared with attribution studies using extended observations back to 1950 but only for regions where stations have 70% data, additionally about a billion people to benefit from attribution information to loss-and-damage negotiations (Thompson and Otto, 2015) and climate change litigation.

A list of the CMIP6 model simulations used in the analysis is presented in Table 1. All-forcing and natural-only forcing simulations of daily maximum and minimum temperatures from CMIP6 models are accessed from the Earth grid federation website via the Center for Environmental Data Analysis (CEDA) node (https://esgf-index1.ceda.ac.uk/search/cmip6-ceda/). Natural-only forcing simulations are available until 2020; historical all-forcing simulations are only available until 2014, and are extended to 2020 using the highest-emissions scenario (SSP5-8.5) simulations. We used CMIP6 models that had both natural-only and all-forcing simulations available over the extent of our analysis period. Although additional all-forcing simulations have been recently released, only a few models had natural-only forcing simulations at the time of this study. For our analysis, natural-only forcing simulations are subtracted from the all-forcing simulations of the respective models to obtain anthropogenic-only forcing simulations.

2.2. Calculation of temperature extremes

Temperature extremes are defined as exceedances of percentile-based thresholds. The 10th and 90th percentiles are computed for both daily maximum and daily minimum temperatures using all years in the analysis period 1981-2020. Using the full 40-yr timeseries as the reference period, and applying a moderate 15-day smoothing window to the thresholds, ensures homogeneity and robustness of exceedance rate estimates across regions (Zhang et al., 2005). The frequency of cold extremes is quantified as the percentage of days below the 10th percentile of daily minimum (TN10) and maximum (TX10) temperatures, while that of hot extremes is the percentage of days exceeding the 90th percentile of daily minimum (TN90) and maximum (TX90) temperatures. These extremes are analyzed over extended seasons: boreal summer from April to September (AMJJAS), and boreal winter from October to March (ONDJFM). The indices are computed for the BEST observational data, reanalysis data as well as the natural-only forced simulations and anthropogenic-only forced simulations of the CMIP6 climate models.

The computation of daily temperature extremes is performed at the grid point level after having regridded all models to a $1^\circ \times 1^\circ$ grid. Dimension reduction is applied to indices computed from both the observations (Y) and simulated forcings (X_i) by decadal and regional averaging. Cosine weighting of latitudes is used in regional averaging, as we analyze several regions: global, the northern hemisphere, the southern hemisphere, and an additional 12 regions over the continents (see Table 2 and Fig. 1). This follows earlier literature (Zwiers et al., 2011; Morak et al., 2013; Zhang et al., 2013; IPCC, 2014) using large scale regions to track the detection of changes from global to hemispheric to large regional scales. The regions are large enough to ensure a high signal-to-noise ratio and robustness of results. A one percent change per decade in the occurrence of extremes in the extended AMJJAS and ONDJFM seasons is equivalent to 1.83 and 1.82 days per decade, respectively.

Table 1
List of the climate models and number of simulations analyzed for each of the different forcings.

Models	ALL	NAT	ANT
ACCESS-ESM1	2	2	2
BCC-CSM2	1	3	1
CanESM5	10	10	10
CNRM-CM6	3	3	3
GFDL- ESM4	1	1	1
IPSL- CM6A	1	1	1
MIROC6	50	50	50
MRI- ESM2	1	1	1

2.3. Attribution method

For the attribution of the causes of changes in temperature extremes we apply a statistical approach to climate change detection and attribution by Ribes et al. (2017) based on the CMIP6 model ensemble of opportunity. The assumption in most fingerprint attribution methods is that the spatiotemporal pattern of response to forcings is constrained by understanding of physical processes, while the more uncertain magnitude of the response is estimated from observations using scaling factors. However, Hegerl and Zwiers (2011) discuss that a multi-model approach addresses climate models' uncertainties only to some degree, and substantial uncertainty exists also in the space-time pattern of response, particularly, in response to aerosols. Atmospheric circulation patterns, large-scale feedbacks, and large uncertainty in the forcings can also influence the spatiotemporal response patterns at regional and local spatial scales (Ribes et al., 2017; Suarez-Gutierrez et al., 2020; IPCC, 2021). Bayesian methods can address response uncertainty (Schurer et al., 2018), but are computer intensive and require prior information. In this study, we use a new method (Ribes et al., 2017) that addresses both the uncertainty in the pattern and magnitude of the fingerprint, and assumes that the true observed response is within the range of climate model simulated responses.

The method accounts for model uncertainty in both amplitude and patterns of response (arising from representation and parameterization of processes in the climate system), excluding sampling uncertainty, by

Table 2
Definition of regions used to assess the contribution of anthropogenic climate change to changes in temperature extremes (adapted from Zwiers et al., 2011; Morak et al., 2013; Zhang et al., 2013; IPCC, 2014).

#	Acronym	Name of region	Lat	Lon
1	GLOB	Global	All	All
2	NH	Northern Hemisphere	0–90 N	All
3	SH	Southern Hemisphere	90S–0 N	All
4	WNA	Western North America	25–55 N	135–100 W
5	ENA	Eastern North America	25–55 N	100–45 W
6	NNAM	Northern North America	55–75 N	165–45 W
7	SAM	Southern America	60 S–5 N	100–40 W
8	EU	Europe	35–75 N	10 W–40 E
9	NAS	Northern Asia	45–80 N	10 E–180
10	SAS	Southern Asia	10–45 N	40 E–180
11	NAF	Northern Africa	15–30 N	20 W–40 E
12	WAF	Western Africa	15 S–15 N	20 W–20 E
13	EAF	Eastern Africa	15 S–15 N	20–55 E
14	SAF	Southern Africa	40–10 S	0–55 E
15	AUS	Australia New Zealand	60–10 S	100 E–180

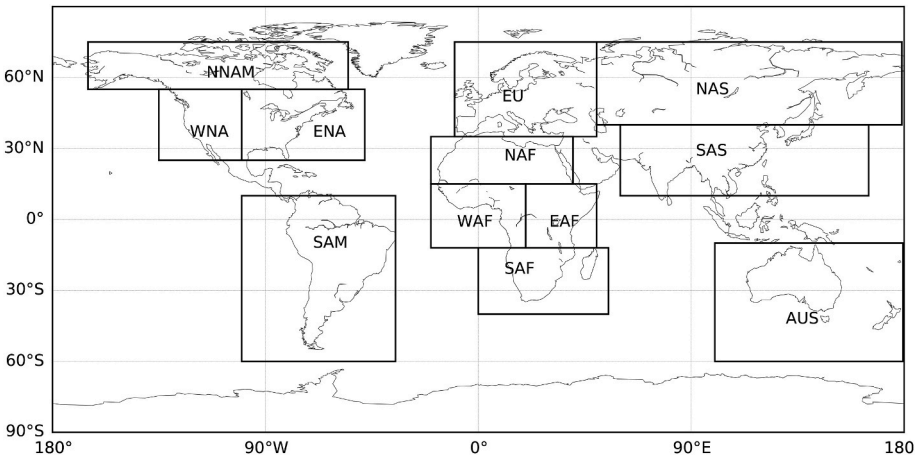

Fig. 1. Definition of regions used to assess the contribution of anthropogenic climate change to changes in temperature extremes. Adapted from literature (Zwiers et al., 2011; Morak et al., 2013; Zhang et al., 2013; IPCC, 2014).

estimating the true simulated response of the climate system to forcings from observations. The method assumes a "models are statistically indistinguishable from the truth paradigm, where the difference between any given model and the truth has the same distribution as the difference between any pair of models" (Ribes et al., 2017). The method addresses models' uncertainties by decomposing the noise term in the true simulated responses to internal climate variability and model uncertainty. Note that the latter may also include forcing uncertainty, to the extent that the CMIP6 ensemble samples it. This method is based on the following statistical model:

$$Y^* = \sum_{i=1}^{n_f} X_i^* \tag{1}$$

$$Y = Y^* + \varepsilon_Y \tag{2}$$

$$X_i = X_i^* + \varepsilon_{X_i} \tag{3}$$

where Y^* is the true response of the climate system to the sum of all external forcings in Eq. (1). X_i^* is the true response of the climate system to an individual forcing i with n_f the number of forcings considered. Y denotes the observations in Eq. (2). X_i in Eq. (3) is the simulated response to forcing i. While the noise term $\varepsilon_Y \sim N(0, \Sigma_Y)$ denotes the observational error and internal variability, the term $\varepsilon_{X_i} \sim N(0, \Sigma_{Xi})$ denotes the uncertainty in model simulations that arises from internal variability, forcing uncertainty, and climate model uncertainty, with Σ_Y and Σ_{Xi} denoting the covariance matrices of observations and model simulations, respectively. Regularization is applied to provide a better estimate of the sample covariance matrices, as demonstrated by Ribes et al. (2009, 2017).

The observed (Y) and simulated (X_i) responses of the climate and their estimated uncertainties are used to estimate true observed (Y^*) and true simulated (X_i^*) forcings using maximum likelihood estimators and sampling uncertainty due to internal variability in that estimate. In order to diagnose the implications for causes of longer-term climate change, the algorithm of Ribes et al. (2017) applies linear trends. Thus, our analysis results in regional change in indices, and their uncertainty from the estimated true Y^* and X_i^*. The uncertainty ranges of the trends are estimated using 1 000 random samples that cover the range of signals consistent with observations.

The internal variability estimate used in the analysis is based on the difference of individual ensemble members from the ensemble mean, rescaled by $\sqrt{(n/n\text{-}1)}$ where n is number of ensemble members (e.g., Ribes et al., 2013; Gillett et al., 2021).

The consistency of the observed trends with internal climate variability has been assessed using a Chi-square test (Ribes et al., 2017; de Abreu et al., 2019). The observed trends and internal climate variability all passed the consistency test. Details of the method is presented in Ribes et al. (2017) and its implementations in a Python package (https://github.com/rafaelcabreu/attribution) is presented in de Abreu et al. (2019).

3. Results

3.1. Observed changes in temperature extremes and in simulated forcings by CMIP6 models

3.1.1. Detected changes in cold and hot extremes

The robustness assessment of BEST data set results followed a two-step procedure. First, we computed indices from observational BEST, and 20C, ERA5 and JRA55 reanalysis data sets for the available respective periods, and computed correlation coefficients between regionally averaged indices of BEST and the reanalysis data sets. Second, we compared detected changes in temperature extremes from BEST with those from ERA5 and JRA55 reanalysis data sets for the period 1981-2020. When changes are detectable in BEST and all the reanalysis data sets, we consider results robust.

The high correlation coefficients (S1) show that BEST is well in agreement with the 20C, ERA5 and JRA55 reanalysis data sets for most of the indices and regions, although there is less agreement over regions in the Southern Hemisphere particularly for regions in Africa. This may be in part due to sparse data over Africa which are filled in by statistical methods in BEST and may not capture the true temperature variability and change, and highlights uncertainty in changes over Africa (see also Engdaw et al., 2021).

Observed changes in the frequency of cold and hot temperature extremes, from BEST (in black) and ERA5 (grey) and JRA55 (light grey) data sets, are plotted in Figs. 2 and 3, respectively. Observed changes in the BEST data set are generally similar with those in ERA5 and JRA55, although ERA5 and JRA55 shows a slightly smaller rate of change in some regions. Therefore, in addition to previous studies (Deng et al., 2021; Perkins-Kirkpatrick and Lewis, 2020; Sippel et al., 2020) which used BEST for detection and attribution, our robustness assessments indicate that BEST agrees with 20C, ERA5 and JRA55 reanalysis data sets. We focus on results using the BEST data set for detection and attribution in the following sections, and discuss where detection and attribution results are different if using ERA5 and JRA55.

Changes in cold temperature extremes computed from BEST data are shown in Fig. 2. Changes are clearly detectable in the inspected extreme indices for all regions and both seasons. Cold extreme temperature indices (TN10 and TX10) show detectable decreasing trends in all

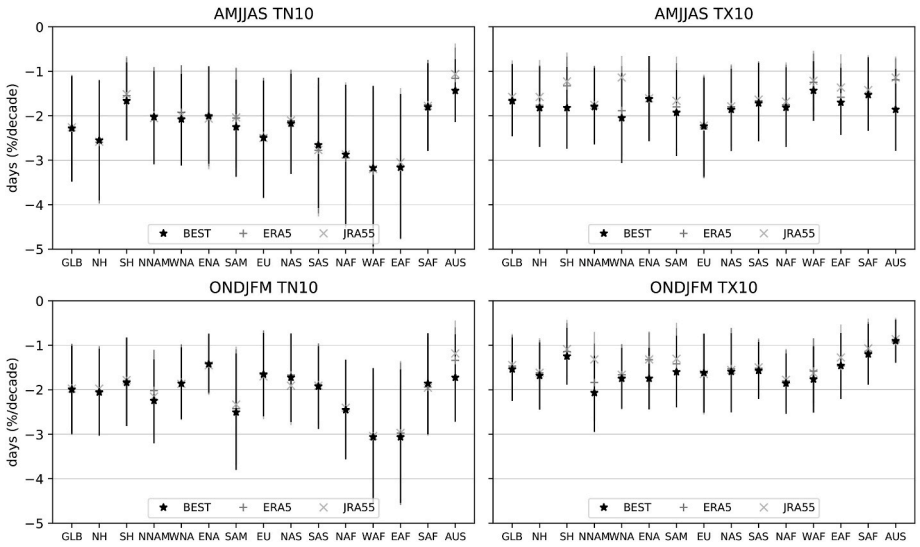

Fig. 2. Changes in cold temperature extreme indices (TN10 and TX10) during 1981-2020 for AMJJAS and ONDJFM seasons, shown for the investigated regions using observational BEST (black), ERA5 (grey) and JRA55 (light grey) reanalysis data sets. Error bars show 95 percentile confidence intervals.

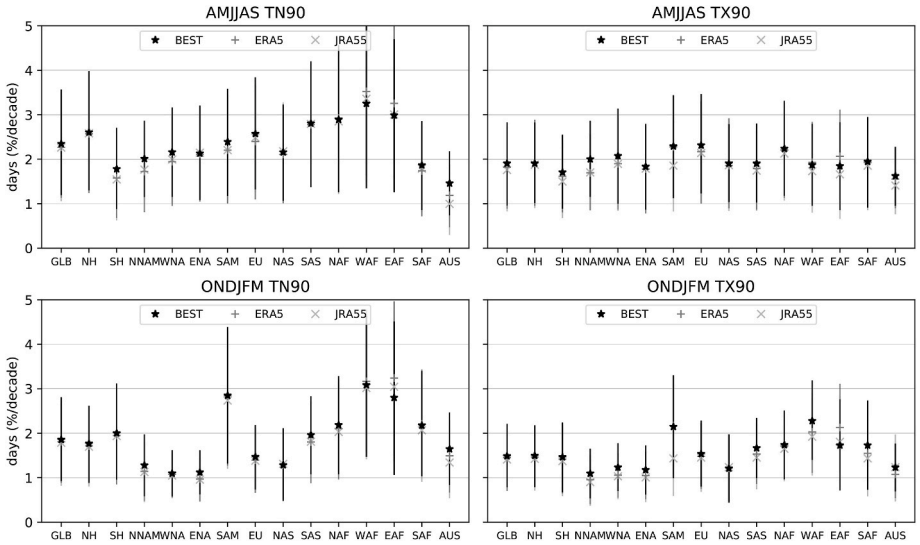

Fig. 3. Changes in hot temperature extreme indices (TN90 and TX90) during 1981-2020 for AMJJAS and ONDJFM seasons, shown for the investigated regions using observational BEST (black), ERA5 (grey) and JRA55 (light grey) reanalysis data sets. Error bars show 95 percentile confidence intervals.

regions and seasons, with larger decadal trends in AMJJAS than in the ONDJFM season. In addition to this, the variability of cold temperature extremes during AMJJAS is higher than that of respective indices in ONDJFM. Comparison of the indices shows that daytime cold extremes (TX10) have less variability than nighttime cold extremes (TN10) (not shown).

All regions (see Table 2 for abbreviations of regions) show more than 2% (3.5 days) per decade decrease in TN10, except SH, SAF, and AUS. Regions over Africa (WAF and EAF) experienced the highest decrease of more than 3% (5.5 days) per decade in TN10, and this behavior is generally robust against using ERA5 and JRA55 data sets (Fig. 2). All regions experienced a decrease of 1–2% (1.8–3.5 days) per decade in TX10 during AMJJAS while EU shows a decrease of more than 2.3% (4.2 days) per decade. During ONDJFM, cold extremes showed a decrease of more than 1.4% (2.5 days) per decade in all regions, the NH, NNAM, SAM NAF, WAF and EAF regions show even 2–3.1% (3.5–5.6 days) per decade decrease in TN10. The decadal trend in TX10 ranges between −0.9 and −2% (−1.6 to −3.6 days) per decade in all regions. The lowest rate of decrease in cold extreme indices (regions) is observed over TN10 (AUS), TX10 (WAF) during AMJJAS and TN10 (ENA), TX10 (AUS) during ONDJFM. Note that with warming the frequency of cold days decreases, and trends will saturate when values below the climatological 10th percentile no longer occur. We also note that space-time averaging results using large regions and trends will ensure that data are reasonably close to normally distributed.

Hot extreme temperature indices (TN90 and TX90) from BEST in Fig. 3 show observed increasing decadal trends, in all regions and both seasons. Most regions experienced a higher than 2% (3.5 days) per decade increase in TN90 during AMJJAS. In the SH, SAF, and AUS, the observed increase is a bit smaller. The African regions NAF, WAF and EAF experienced the highest decadal trend of up to 3.2% (5.8 days) for TN90.1.7%, about 3 days (SH and AUS) is the lowest trend per decade of TX90 in AMJJAS while WNA, SAM, EU, SAS, and NAF experienced more than 2% (3.5 days) increase per decade. Decadal trends of hot temperature extremes observed in ONDJFM are slightly lower than in AMJJAS over the respective regions. The frequency increase of TN90 ranges from 1% (1.8 days) per decade in WNA and ENA to 3.1% (5.7 days) in WAF. For TX90, the highest decadal trend is observed over WAF with 2.2% (4

days) increase per decade. TX90 trends are 1–2.2% (1.8–4 days) during ONDJFM. Due to the seasonal cycle, SH, SAF, SAM are regions where observed changes in cold extremes in ONDJFM are higher than AMJJAS.

The magnitude of change of temperature extremes in AMJJAS is higher than in ONDJFM. In both seasons, nighttime extreme temperature indices (TN10 and TN90) showed higher decadal trends than those of daytime extreme indices (TX10 and TX90). The highest decadal change in temperature extreme indices is observed over regions in Africa; NAF, WAF and EAF. This implies that climate change is adversely affecting less developed and vulnerable regions which in turn increases vulnerability. However, in these regions there is also substantial data uncertainty, reflected also in larger differences to results from reanalysis data.

3.1.2. Temperature extremes in forcings simulated by CMIP6 models

Time series of extreme temperature indices for AMJJAS are shown in Figs. 4–7 for the different analyzed regions. Note that the equivalent ONDJFM time series are shown in Supplementary Figs. S2–S5. The thick lines show the BEST observations (black) and the multi-model means of the natural-only (blue) and anthropogenic-only (red) forced CMIP6 climate model simulations. Cold extreme temperature indices, TN10 (Fig. 4) and TX10 (Fig. 5), computed from anthropogenically forced simulations show a decrease over the inspected period similar to the observations, while the changes in cold extremes due to natural forcings are very weak. The natural-only simulations clearly capture the short-term cooling signals due to volcanic eruptions – El Chichon early 1980 and Pinatubo in early 1990 – in all regions with different magnitude and lifespan. Volcanic eruptions contribute to larger signal variability of cold extremes in natural-only forced simulations. The variability of cold night extremes (TN10) is higher than that of cold day extremes (TX10) in the climate forcing simulations. Indices of forced simulations show higher variability over land in the northern hemisphere and in regions located north of the equator. In ONDJFM, cold extreme temperature indices show relatively less variability than the AMJJAS cold extremes, TN10 in Fig. S2 and TX10 in Fig. S3.

Hot temperature extremes during night (TN90) and during day (TX90) are shown in Figs. 6 and 7, respectively, for AMJJAS. Hot temperature extremes computed from observations and anthropogenic-forced simulations clearly show increasing trend signals over time in all regions. The influence of both volcanic eruptions is evident, with the reduction in incoming radiation cooling down hot extremes computed from natural-only simulations. The variability in nighttime hot extremes (TN90) is higher than in daytime hot extremes (TX90) in the climate simulations. The variability in TN90 strongly varies from region to region. Changes in hot temperature extremes are smaller in ONDJFM compared to AMJJAS in all regions, for TN90 in Fig. S4 and TX90 in Fig. S5.

3.2. Attribution of causes to changing temperature extremes

Results of the attribution analysis on the causes of changing cold extremes and hot extremes are presented in Figs. 8 and 9, respectively, showing the contribution of anthropogenic (in red) and natural forcings (in blue) to the observed changes (in black). Changes are assessed based on observations of the BEST data set, which has been used also by other studies to evaluate climate models, to assess observed changes and to attribute detected changes (Deng et al., 2021; Perkins-Kirkpatrick and Lewis, 2020; Sippel et al., 2020) over all regions of the world. The period of analysis we used, 1981-2020, is the time of best coverage of meteorological stations. In addition, for assessing the robustness of results from BEST data, we conducted the analysis for ERA5 and JRA55 reanalysis data sets, and found the results consistent (Figs. 8 and 9). For indices (in a region) computed from natural forcing, we consider statistical significance when using observational BEST and at least one of the two reanalysis data sets to state natural forcing is robustly detectable, while anthropogenic forcing is robustly detectable in all data sets for all indices and regions. However, we need to point out that interpreting attribution results over regions known for data scarcity should be made with care.

The observed changes in all temperature extremes in this analysis can be attributed to anthropogenic forcing, which contribute with a large magnitude to decadal trends in both seasons and all regions. The magnitudes vary with indices, regions, and seasons.

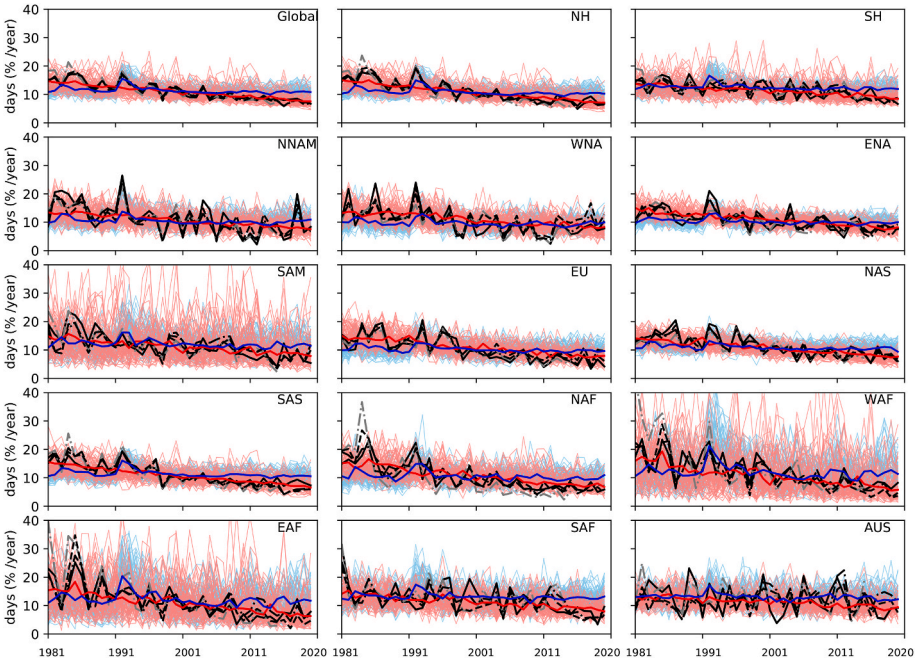

Fig. 4. TN10 from BEST observations (solid black), ERA5 (dashed black), JRA55 (dash-dotted black), 20C (dash-dotted grey) reanalyses and multi-model means (thick, colored) of the CMIP6 simulations with anthropogenic (red) and natural (blue) forcings shown for the AMJJAS season. (For interpretation of the references to color in this figure legend, the reader is referred to the Web version of this article.)

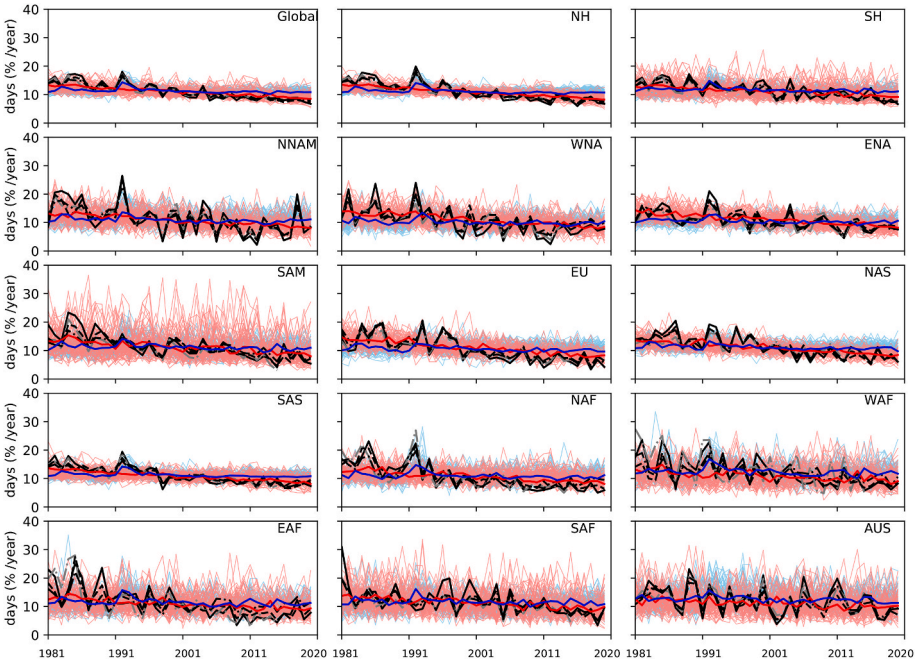

Fig. 5. TX10 from BEST observations (solid black), ERA5 (dashed black), JRA55 (dash-dotted black), 20C (dash-dotted grey) reanalyses and multi-model means (thick, colored) of the CMIP6 simulations with anthropogenic (red) and natural (blue) forcings shown for the AMJJAS season. (For interpretation of the references to color in this figure legend, the reader is referred to the Web version of this article.)

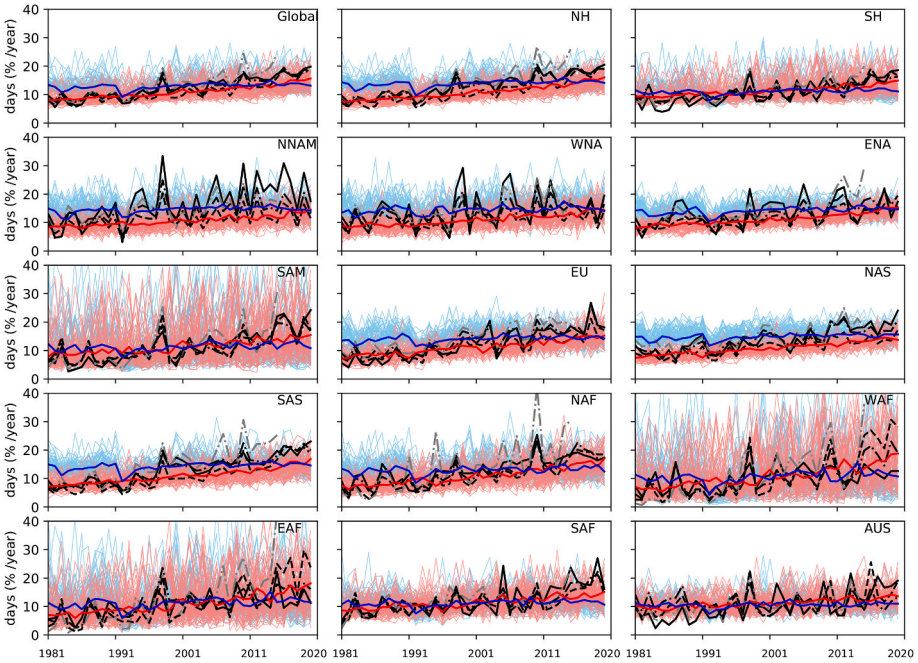

Fig. 6. TN90 from BEST observations (solid black), ERA5 (dashed black), JRA55 (dash-dotted black), 20C (dash-dotted grey) reanalyses and multi-model means (thick, colored) of the CMIP6 simulations with anthropogenic (red) and natural (blue) forcings shown for the AMJJAS season. (For interpretation of the references to color in this figure legend, the reader is referred to the Web version of this article.)

3.2.1. Cold extremes

Anthropogenic forcing is responsible for a more than 1% (1.8 days) per decade change in AMJJAS TN10 in all regions. Regions in different continents experienced human-induced decrease in cold nights, on global-land (1.8%, 3.3 days per decade), Northern America (1.6%, 2.9 days per decade), Europe (2%, 3.7 day per decade), Asia (1.7–2.2%, 3–3.5 days per decade), and Africa (2.5%, 4.5 days per decade). AUS experienced the lowest anthropogenic-induced reduction (1%, 1.8 days per decade). During AMJJAS, the human-induced decrease in TX10 reached 1.3–1.5%, (2.4–2.8 days) per decade for global land and Northern America and 1.2%, 1.5%, 1.7% (2.3, 2.7, 3.2 days) per decade for Africa, Asia, and EU, respectively. The largest anthropogenic contributions, of cold extremes in AMJJAS, are estimated over regions of EU, Asia and Africa. Although the pattern of regional changes of cold extremes during ONDJFM are similar to those in AMJJAS, the contribution of anthropogenic forcing to changes in cold extremes in ONDJFM

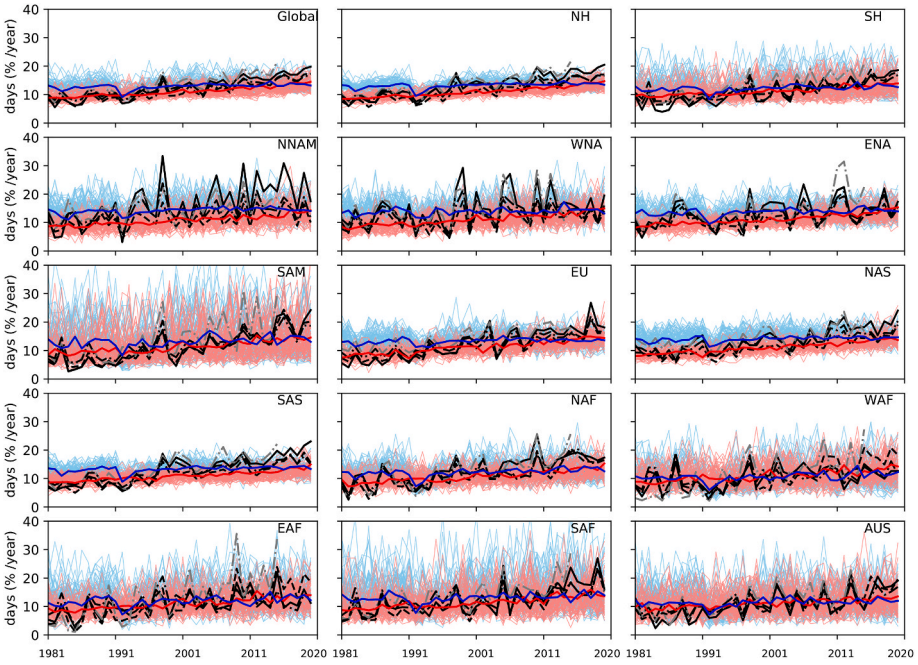

Fig. 7. TX90 from BEST observations (solid black), ERA5 (dashed black), JRA55 (dash-dotted black), 20C (dash-dotted grey) reanalyses, and multi-model means (thick, colored) of the CMIP6 simulations with anthropogenic (red) and natural (blue) forcings shown for the AMJJAS season. (For interpretation of the references to color in this figure legend, the reader is referred to the Web version of this article.)

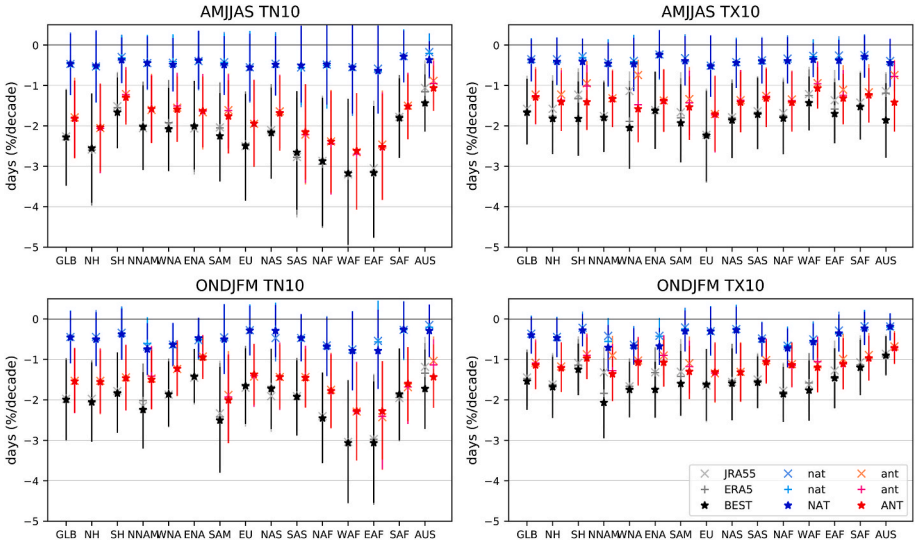

Fig. 8. Contribution of natural (NAT, blue) and anthropogenic (ANT, red) forcings to the total observed changes (from BEST, in black as in Fig. 2) in cold temperature extreme indices (TN10 and TX10) during 1981-2020 for AMJJAS and ONDJFM seasons, shown for the investigated regions. In addition, changes detected from ERA5 (grey) with natural (sky blue) and anthropogenic (pink) contributions and changes detected from JRA55 (light grey) with natural (light blue) and anthropogenic (orange) contributions are shown. Error bars show 95 percentile confidence intervals. (For interpretation of the references to color in this figure legend, the reader is referred to the Web version of this article.)

is smaller than in AMJJAS as for the total observed change. Anthropogenic contributions for TN10 and TX10 in ONDJFM ranged between 0.9 and 2.3% (1.7–4.1 days) and 0.7–1.4% (1.3–2.5 days) per decade, respectively. When cold extremes of both seasons are compared, cold extremes of the ONDJFM season show narrower uncertainty ranges. Further investigation of cold extremes for five selected regions, based on HadEX3 data availability (NNAM, WNA, ENA, EU, AUS), shows consistent results between our results based on BEST and ERA with results using extremes indices from HadEX3 observations as presented in Fig. S6 of the supplementary material. This supports that results are robust to data uncertainty in well sampled regions.

The contribution of natural forcings ranged between 0.5 and 1.2 days (TN10) and 0.4–1 days (TX10) per decade during AMJJAS, and between 0.2 and 1.4 days (TN10) and 0.4–1.3 days (TX10) per decade decrease during ONDJFM. In ONDJFM, contributions of natural forcings are detectable, although not in all of the regions. Detectable natural forcings are robust to using ERA5 and JRA55 data sets instead. BEST and at least one of the reanalysis data sets (ERA5 and JRA55) agree in the detectable contribution of natural forcings in indices (regions) of ONDJFM's TN10 (NNAM and WNA) and ONDJFM's TX10 (WNA, SAS, NAF, and WAF). Furthermore, all the data sets (BEST, ERA5 and JRA55) agree on the robust detectability of natural forcings in ONDJFM's cold extremes: TN10 in WNA, and TX10 in WNA, SAS, NAF and WAF regions. Results for HadEX3 are consistent on the detectability of natural forcings for TN10 and TX10 in WNA.

3.2.2. *Hot extremes*

The contribution of anthropogenic forcings to hot extremes is the only detectable contributor to hot extremes in many regions, and much higher than the contribution of natural forcings in all regions and both

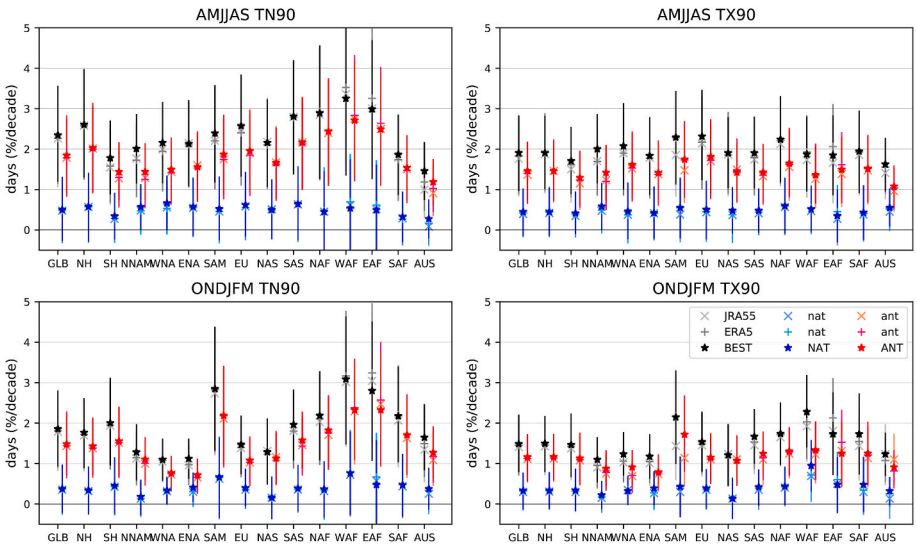

Fig. 9. Contribution of natural (NAT, blue) and anthropogenic (ANT, red) forcings to the total observed changes (from BEST, in black as in Fig. 2) in hot temperature extreme indices (TN90 and TX90) during 1981-2020 for AMJJAS and ONDJFM seasons, shown for the investigated regions. In addition, changes detected from ERA5 (grey) with natural (sky blue) and anthropogenic (pink) contributions and changes detected from JRA55 (light grey) with natural (light blue) and anthropogenic (orange) contributions are shown. Error bars show 95 percentile confidence intervals. (For interpretation of the references to color in this figure legend, the reader is referred to the Web version of this article.)

seasons. The largest anthropogenic forcing contribution is detected in AMJJAS for changes in nighttime extremes as well as in daytime extremes. Also, in ONDJFM, the anthropogenic contribution to changes in nighttime extremes is large.

The anthropogenic contribution to decadal changes in hot extremes is estimated to be 1.2–2.6% (2.2–4.8 days) per decade for TN90, 1–1.8% (2–3.3 days) per decade for TX90 in AMJJAS. In ONDJFM, it is 0.7–2.3% (1.3–4.2 days) per decade for TN90, and 0.7–1.7% (1.3–3.1 days) per decade for TX90. The highest contributions of anthropogenic forcing to decadal changes in hot extremes are 2.6% (4.8 days) per decade for TN90 in WAF, 1.8% (3.3 days) per decade for TX90 in EU during AMJJAS, and during ONDJFM it is 2.3% (4.2 days) per decade for TN90 in WAF and EAF and 1.7% (3 days) per decade for TX90 in SAM.

The highest contribution of anthropogenic forcing is detected in Africa, while Northern America and Australia are continents where the lowest contributions of anthropogenic forcing to decadal changes of extreme temperatures are detected. Over the African continent, the observed decadal changes are large and the highest human-induced increase in temperature extremes is detected. Therefore, much attention is needed in multiple aspects. For Australia, in addition to its warm mean climate, the detected anthropogenic contribution to hot extremes has contributed to an increase in climate-driven extreme events in the recent years. Similar to cold extremes, the uncertainty range of hot extremes in ONDJFM is found smaller than in the AMJJAS season. Furthermore, the results on hot extremes are comparable with those from the HadEX3 data set in the selected regions as well (Fig. S7).

Contributions from natural forcings range over 0.6–1 days per decade in AMJJAS for both hot extreme indices, while it is 0.35–1.8 days per decade for both TN90 and TX90 in ONDJFM. Some detectable contribution of natural forcings to changes in hot extremes are found in AUS for TX90 in AMJJAS, and WAF for TX90 in ONDJFM. Detected natural forcing contributions are about 0.5% (1 day) per decade for both cold and hot extremes, and even smaller in the ONDJFM season.

The anthropogenic-forcing contribution to changes in all temperature extremes is much larger in all regions than the contribution from natural forcings. The contribution of natural forcings is mainly detected in daytime cold temperature extremes. This might predominantly be due to updated solar irradiance and volcanic forcings, which were underestimated in CMIP5 (Ridley et al., 2014; Santer et al., 2014; Lean, 2018; Fyfe et al., 2021), and due to improved variability in CMIP6 models. The attribution results for the changes detected for cold and hot temperature extremes using ERA5 and JRA55 data sets are included in Figs. 8 and 9, respectively, and are qualitatively similar with attribution results based on BEST data set. Observational BEST and at least one of the reanalysis data sets show detectable contribution of natural forcings for indices (regions) of AMJJAS's TX90 (AUS) consistent with HadEX3 results, and of ONDJFM's TX90 (WAF). Consistent detectability is found for HadEX3 for AMJJAS' TX90 (AUS).

In addition, the regional contribution of anthropogenic and natural forcings to changes in TN90 in AMJJAS, based on the BEST data set, is demonstrated using a pie chart in Supplementary Fig. S8. Anthropogenic forcings' contribution is larger in low latitude regions.

4. Conclusion

Temperature extremes observed in the last decades are assessed in observations from BEST data. Statistically significant changes have been detected in cold temperature extremes (TN10 and TX10) and in hot temperatures extremes (TN90 and TX90) over 1981–2020 in both extended AMJJAS and ONDJFM seasons and over all land regions. Overall, extremes (rate of change) show a decrease in TN10 (2-3% per decade), TX10 (1-2% per decade), and an increase in TN90 (2-3% per decade), TX90 (1–2.5% per decade) in the AMJJAS season and slightly less change in the ONDJFM season. Temperature extremes in AMJJAS showed higher decadal trends over tropical regions and the northern hemisphere, and lower trends for regions in the southern hemisphere. Regions in Africa, Asia/EU, and North America experienced the highest decadal changes in temperature extremes.

Our attribution analysis, using CMIP6 climate model simulations, revealed that anthropogenic climate change is clearly the main contributor of detected changes in temperature extremes. High and detectable contributions of human-induced forcing are consistently found for all inspected extreme indices, in all regions and both seasons. The contributions of human-induced climate change for decrease in nighttime cold extremes (TN10) and increase in nighttime hot extremes (TN90) is about 1–2.5% per decade in both seasons, in all regions. While contributions estimated from the same forcing for decrease in daytime cold extremes (TX10) are between 0.7 and 1.7% per decade in both seasons, increase in daytime hot extremes (TX90) are estimated between 1 and 1.8% per decade for AMJJAS and between 0.7 and 1.7% for ONDJFM season. These results are consistent with results from HadEX3 data in selected regions with dense observations.

In addition, our analysis revealed that natural forcings have only contributed to changes in temperature extremes to a minor extent and cannot explain the observed changes. Despite higher rate of changes detected in nighttime temperature extremes (TN10 and TN90), in both seasons and all regions, the contribution of natural forcings is detected predominantly in cold extreme temperatures (TN10 and TX10). The

contributions attributed to natural forcings are about 0.5% (1 day) per decade for both cold and hot extreme indices in AMJJAS, and even smaller for indices in ONDJFM season. The observational BEST and at least one of the reanalysis data sets (ERA5 and JRA55) agree in the robustly detectable contribution of natural forcings in indices (regions) of ONDJFM's TN10 (NNAM and WNA) and ONDJFM's TX10 (WNA, SAS, NAF and WAF), AMJJAS's TX90 (AUS) and ONDJFM's TX90 (WAF). All the data sets agree on the robustly detectable contribution of natural forcings to ONDJFM's TX90 (WAF) and cold extremes of ONDJFM: TN10 in WNA, and TX10 in WNA, SAS, NAF and WAF regions.

In summary, changes in cold (TN10 and TX10) and hot (TN90 and TX90) temperature extremes are detectable in all the regions and both AMJJAS and ONDJFM seasons. Detected changes in observational BEST and ERA5 and JRA55 reanalysis data sets are consistent for most of the regions. Our attribution analysis showed a detectable contribution from natural forcings in several regions, predominantly for daytime cold temperature extremes. Updated temperature data and forcings, and improved variability in CMIP6 models may have increased the detectability of natural forcing contributions. In addition, the agreement among the data sets we used, in some regions, shows the robustness of the detectable small contribution of natural forcings, although they cannot explain observed changes. While natural forcings contribute to the change in extremes in some regions, possibly due to the recovery from the eruption of Mount Pinatubo early in the record, natural forcings alone cannot explain the observed changes in extremes. Our results, based on the improved state-of-the-art CMIP6 models, show that anthropogenic forcings are detectable in all indices for all regions, consistently in all data sets. Furthermore, anthropogenic forcings are the main drivers and have contributed the most to the observed changes in temperature extremes in all regions.

Authors' contribution

MME: Data curation; Formal analysis; Investigation; Methodology; Visualization; Roles/Writing - original draft; Writing - review & editing.

AKS: Conceptualization; Funding acquisition; Resources; Supervision; Visualization; Roles/Writing - review & editing.

GCH: Methodology; supervision; Writing - review & editing.

APB: Methodology; supervision; Writing - review & editing.

Declaration of competing interest

The authors declare that they have no known competing financial interests or personal relationships that could have appeared to influence the work reported in this paper.

Data availability

All the data and code used in this research is indicated available in the acknowledgement section of the manuscript.

Acknowledgements

This work was funded by the Austrian Science Fund (FWF) under Research Grant W1256 (Doctoral Programme Climate Change – Uncertainties, Thresholds and Coping Strategies). Andrew Ballinger was funded by the EUCP project funded by the European Commission's Horizon 2020 programme, Grant Agreement number 776613, and Gabriele Hegerl by the NERC grant 'EMERGENCE', NE/S004645/1. The authors acknowledge the Berkeley Earth Surface Temperature (BEST), the European Centre for Medium-Range Weather Forecasts (ECMWF), National Oceanic Atmospheric Administration (NOAA) for making accessible the BEST, ERA5 and 20C data sets. BEST data are available at http://berkeleyearth.org/. The 20C, ERA5, JRA55 and HadEX3 data sets are available at https://psl.noaa.gov/data/20thC_Rean/, https://cds.climate.copernicus.eu/cdsapp#!/home, https://jra.kishou.go.jp/JRA-55/index_en.html, and https://www.metoffice.gov.uk/hadobs/hadex3/, respectively. We also acknowledge the climate modelling groups for making their respective simulations publicly available through the Center for Environmental Data Analysis (CEDA) node at https://esgf-index1.ceda.ac.uk/search/cmip6-ceda/. We also acknowledge Rafael de Abreu for making the Python package freely available at https://github.com/rafaelcabreu/attribution.

Appendix A. Supplementary data

Supplementary data to this article can be found online at https://doi.org/10.1016/j.wace.2023.100548.

References

Alexander, L.V., 2016. Global observed long-term changes in temperature and precipitation extremes: a review of progress and limitations in IPCC assessments and beyond. Weather Clim. Extrem. 11, 4–16. https://doi.org/10.1016/j.wace.2015.10.007.

Alexander, L.V., Zhang, X., Peterson, T.C., Caesar, J., Gleason, B., Klein Tank, A.M.G., et al., 2006. Global observed changes in daily climate extremes of temperature and precipitation. J. Geophys. Res. Atmos. 111 (D5) https://doi.org/10.1029/2005JD006290.

Allen, M., 2003. Liability for climate change. Nature 421 (6926), 891–892. https://doi.org/10.1038/421891a.

Almazroui, M., Ashfaq, M., Islam, M.N., Rashid, I.U., Kamil, S., Abid, M.A., et al., 2021. Assessment of CMIP6 performance and projected temperature and precipitation changes over south America. Earth Systems and Environment 1–29. https://doi.org/10.1007/s41748-021-00233-6.

Chen, H., Sun, J., Lin, W., Xu, H., 2020. Comparison of CMIP6 and CMIP5 models in simulating climate extremes. Sci. Bull. 65 (17), 1415–1418. https://doi.org/10.1016/j.scib.2020.05.015.

Christidis, N., Jones, G.S., Stott, P.A., 2015. Dramatically increasing chance of extremely hot summers since the 2003 European heatwave. Nat. Clim. Change 5 (1), 46–50. https://doi.org/10.1038/nclimate2468.

Christidis, N., McCarthy, M., Stott, P.A., 2020. The increasing likelihood of temperatures above 30 to 40° C in the United Kingdom. Nat. Commun. 11 (1), 1–10. https://doi.org/10.1038/s41467-020-16834-0.

Cowan, T., Purich, A., Perkins, S., Pezza, A., Boschat, G., Sadler, K., 2014. More frequent, longer, and hotter heat waves for Australia in the twenty-first century. J. Clim. 27 (15), 5851–5871.

De Abreu, R.C., Tett, S.F.B., Schurer, A., Rocha, H.R., 2019. Attribution of detected temperature trends in Southeast Brazil. Geophys. Res. Lett. 46 (14), 8407–8414. https://doi.org/10.1029/2019GL083003.

Deng, X., Perkins-Kirkpatrick, S.E., Lewis, S.C., Ritchie, E.A., 2021. Evaluation of extreme temperatures over Australia in the historical simulations of CMIP5 and CMIP6 models. Earth's Future 9 (7), e2020EF001902. https://doi.org/10.1029/2020EF001902.

Di Luca, A., Pitman, A.J., de Elía, R., 2020. Decomposing temperature extremes errors in CMIP5 and CMIP6 models. Geophys. Res. Lett. 47 (14), e2020GL088031 https://doi.org/10.1029/2020GL088031.

Dittus, A.J., Karoly, D.J., Lewis, S.C., Alexander, L.V., Donat, M.G., 2016. A multiregion model evaluation and attribution study of historical changes in the area affected by temperature and precipitation extremes. J. Clim. 29 (23), 8285–8299. https://doi.org/10.1175/JCLI-D-16-0164.1.

Donat, M.G., Alexander, L.V., Yang, H., Durre, I., Vose, R., Dunn, R.J., et al., 2013. Updated analyses of temperature and precipitation extreme indices since the beginning of the twentieth century: the HadEX2 dataset. J. Geophys. Res. Atmos. 118 (5), 2098–2118. https://doi.org/10.1002/jgrd.50150.

Dong, B., Sutton, R.T., Shaffrey, L., 2017. Understanding the rapid summer warming and changes in temperature extremes since the mid-1990s over Western Europe. Clim. Dynam. 48 (5–6), 1537–1554. https://doi.org/10.1007/s00382-016-3158-8.

Dong, S., Sun, Y., Aguilar, E., Zhang, X., Peterson, T.C., Song, L., Zhang, Y., 2018. Observed changes in temperature extremes over Asia and their attribution. Clim. Dynam. 51 (1), 339–353. https://doi.org/10.1007/s00382-017-3927-z.

Duan, J., Ma, Z., Wu, P., Xoplaki, E., Hegerl, G., Li, L., Luterbacher, J., 2019. Detection of human influences on temperature seasonality from the nineteenth century. Nat. Sustain. 2 (6), 484–490. https://doi.org/10.1038/s41893-019-0276-4.

Dunn, R.J., Alexander, L.V., Donat, M.G., Zhang, X., Bador, M., Herold, N., Bin Hj Yussof, M.N.A., 2020. Development of an updated global land in situ-based data set of temperature and precipitation extremes: HadEX3. J. Geophys. Res. Atmos. 125 (16), e2019JD032263 https://doi.org/10.1029/2019JD032263.

Engdaw, M.M., Ballinger, A.P., Hegerl, G.C., Steiner, A.K., 2021. Changes in temperature and heat waves over Africa using observational and reanalysis data sets. Int. J. Climatol. 1–16. https://doi.org/10.1002/joc.7295.

Eyring, V., Bony, S., Meehl, G.A., Senior, C.A., Stevens, B., Stouffer, R.J., Taylor, K.E., 2016. Overview of the coupled model Intercomparison project phase 6 (CMIP6) experimental design and organization. Geosci. Model Dev. (GMD) 9 (5), 1937–1958. https://doi.org/10.5194/gmd-9-1937-2016, 2016.

Eyring, V., Gillett, N.P., Achuta Rao, K.M., Barimalala, R., Barreiro Parrillo, M., Bellouin, N., Cassou, C., Durack, P.J., Kosaka, Y., McGregor, S., Min, S., Morgenstern, O., Sun, Y., 2021. Human influence on the climate system. In: Masson-

Delmotte, V., Zhai, P., Pirani, A., Connors, S.L., Péan, C., Berger, S., Caud, N., Chen, Y., Goldfarb, L., Gomis, M.I., Huang, M., Leitzell, K., Lonnoy, E., Matthews, J. B.R., Maycock, T.K., Waterfield, T., Yelekçi, O., Yu, R., Zhou, B. (Eds.), Climate Change 2021: the Physical Science Basis. Contribution of Working Group I to the Sixth Assessment Report of the Intergovernmental Panel on Climate Change. Cambridge University Press, Cambridge, United Kingdom and New York, NY, USA, pp. 423–552. https://doi.org/10.1017/9781009157896.005.

Fischer, E.M., Knutti, R., 2015. Anthropogenic contribution to global occurrence of heavy-precipitation and high-temperature extremes. Nat. Clim. Change 5 (6), 560–564. https://doi.org/10.1038/nclimate2617.

Fyfe, J.C., Kharin, V.V., Santer, B.D., Cole, J.N., Gillett, N.P., 2021. Significant impact of forcing uncertainty in a large ensemble of climate model simulations. Proc. Natl. Acad. Sci. USA 118 (23), e2016549118. https://doi.org/10.1073/pnas.2016549118.

Gillett, N.P., Kirchmeier-Young, M., Ribes, A., Shiogama, H., Hegerl, G.C., Knutti, R., et al., 2021. Constraining human contributions to observed warming since the pre-industrial period. Nat. Clim. Change 11 (3), 207–212. https://doi.org/10.1038/s41558-020-00965-9.

Hegerl, G., Zwiers, F., 2011. Use of models in detection and attribution of climate change. Wiley interdisciplinary reviews: Clim. Change 2 (4), 570–591. https://doi.org/10.1002/wcc.121.

Hegerl, G.C., voN StoRcH, H., Hasselmann, K., Santer, B.D., Cubasch, U., Jones, P.D., 1996. Detecting greenhouse-gas-induced climate change with an optimal fingerprint method. J. Clim. 9 (10), 2281–2306. https://doi.org/10.1175/1520-0442(1996)009<2281:DGGICC>2.0.CO;2.

Hegerl, G.C., Hasselmann, K., Cubasch, U., Mitchell, J.F., Roeckner, E., Voss, R., Waszkewitz, J., 1997. Multi-fingerprint detection and attribution analysis of greenhouse gas, greenhouse gas-plus-aerosol and solar forced climate change. Clim. Dynam. 13 (9), 613–634.

Hegerl, G.C., Brönnimann, S., Cowan, T., Friedman, A.R., Hawkins, E., Iles, C., et al., 2019. Causes of climate change over the historical record. Environ. Res. Lett. 14 (12), 123006 https://doi.org/10.1088/1748-9326/ab4557.

Hersbach, H., Bell, B., Berrisford, P., Hirahara, S., Horanyi, A., Muñoz-Sabater, J., Nicolas, J., Peubey, C., Radu, R., Schepers, D., Simmons, A., Soci, C., Abdalla, S., Abellan, X., Balsamo, G., Bechtold, P., Biavati, G., Bidlot, J., Bonavita, M., Chiara, G. D., Dahlgren, P., Dee, D., Diamantakis, M., Dragani, R., Flemming, J., Forbes, R., Fuentes, M., Geer, A., Haimberger, L., Healy, S., Hogan, R.J., Holm, E., Janiskova, M., Keeley, S., Laloyaux, P., Lopez, P., Lupu, C., Radnoti, G., deRosnay, P., Rozum, I., Vamborg, F., Villaume, S., Thépaut, J.-N., 2020. The ERA5 global reanalysis. Q. J. R. Meteorol. Soc. 146, 1999–2049. https://doi.org/10.1002/qj.3803.

Hu, T., Sun, Y., Zhang, X., Min, S.K., Kim, Y.H., 2020. Human influence on frequency of temperature extremes. Environ. Res. Lett. 15 (6), 064014 https://doi.org/10.1088/1748-9326/ab8497.

IPCC, 2014. Climate change 2014: impacts, adaptation, and vul-nerability. Part B: regional aspects. In: Barros, V.R., Field, C.B., Dokken, D.J., Mastrandrea, M.D., Mach, K.J., Bilir, T.E., Chatterjee, M., Ebi, K.L., Estrada, Y.O., Genova, R.C., Girma, B., Kissel, E.S., Levy, A.N., MacCracken, S., Mastrandrea, P.R., White, L.L. (Eds.), Contribution of Working Group II to the Fifth Assessment Report of the Intergov-ernmental Panel on Climate Change. Cambridge University Press, Cambridge, United King-dom and New York, NY, USA, p. 688.

IPCC, 2021. In: Masson-Delmotte, V., Zhai, P., Pirani, A., Connors, S.L., Péan, C., Berger, S., Caud, N., Chen, Y., Goldfarb, L., Gomis, M.I., Huang, M., Leitzell, K., Lonnoy, E., Matthews, J.B.R., Maycock, T.K., Waterfield, T., Yelekçi, O., Yu, R., Zhou, B. (Eds.), Climate Change 2021: the Physical Science Basis. Contribution of Working Group I to the Sixth Assessment Report of the Intergovernmental Panel on Climate Change. Cambridge University Press, Cambridge, United Kingdom and New York, NY, USA. https://doi.org/10.1017/9781009157896 (in press).

Jézéquel, A., Dépoues, V., Guillemot, H., Rajaud, A., Trolliet, M., Vrac, M., et al., 2020. Singular extreme events and their attribution to climate change: a climate service–centered analysis. Weather, Climate, and Society 12 (1), 89–101.

Kim, Y.H., Min, S.K., Zhang, X., Sillmann, J., Sandstad, M., 2020. Evaluation of the CMIP6 multi-model ensemble for climate extreme indices. Weather Clim. Extrem. 29, 100269 https://doi.org/10.1016/j.wace.2020.100269.

Kobayashi, S., Ota, Y., Harada, Y., Ebita, A., Moriya, M., Onoda, H., Onogi, K., Kamahori, H., Kobayashi, C., Endo, H., Miyaoka, K., 2015. The JRA-55 reanalysis: general specifications and basic characteristics. J. Meteorological Soc. Japan. Series. II 93 (1), 5–48. https://doi.org/10.2151/jmsj.2015-001.

Lean, J.L., 2018. Observation-based detection and attribution of 21st century climate change. Wiley Interdisciplinary Reviews: Clim. Change 9 (2), e511. https://doi.org/10.1002/wcc.511.

Li, C., Fang, Y., Caldeira, K., Zhang, X., Diffenbaugh, N.S., Michalak, A.M., 2018. Widespread persistent changes to temperature extremes occurred earlier than predicted. Sci. Rep. 8 (1), 1–8. https://doi.org/10.1038/s41598-018-19288-z.

Li, C., Zwiers, F., Zhang, X., Li, G., Sun, Y., Wehner, M., 2020. Changes in annual extremes of daily temperature and precipitation in CMIP6 models. J. Clim. 1–61. https://doi.org/10.1175/JCLI-D-19-1013.1.

Masud, B., Cui, Q., Ammar, M.E., Bonsal, B.R., Islam, Z., Faramarzi, M., 2021. Means and extremes: evaluation of a CMIP6 multi-model ensemble in reproducing historical climate characteristics across alberta, Canada. Water 13 (5), 737. https://doi.org/10.3390/w13050737.

Morak, S., Hegerl, G.C., Kenyon, J., 2011. Detectable regional changes in the number of warm nights. Geophys. Res. Lett. 38 (17) https://doi.org/10.1029/2011GL048531.

Morak, S., Hegerl, G.C., Christidis, N., 2013. Detectable changes in the frequency of temperature extremes. J. Clim. 26 (5), 1561–1574. https://doi.org/10.1175/JCLI-D-11-00678.1.

Perkins-Kirkpatrick, S.E., Lewis, S.C., 2020. Increasing trends in regional heatwaves. Nat. Commun. 11 (1), 1–8. https://doi.org/10.1038/s41467-020-16970-7.

Ribes, A., Azaïs, J.M., Planton, S., 2009. Adaptation of the optimal fingerprint method for climate change detection using a well-conditioned covariance matrix estimate. Clim. Dynam. 33 (5), 707–722. https://doi.org/10.1007/s00382-009-0561-4.

Ribes, A., Planton, S., Terray, L., 2013. Application of regularised optimal fingerprinting to attribution. Part I: method, properties and idealised analysis. Clim. Dynam. 41 (11–12), 2817–2836. https://doi.org/10.1007/s00382-013-1735-7.

Ribes, A., Zwiers, F.W., Azais, J.M., Naveau, P., 2017. A new statistical approach to climate change detection and attribution. Clim. Dynam. 48 (1), 367–386. https://doi.org/10.1007/s00382-016-3079-6.

Ridley, D.A., Solomon, S., Barnes, J.E., Burlakov, V.D., Deshler, T., Dolgii, S.I., et al., 2014. Total volcanic stratospheric aerosol optical depths and implications for global climate change. Geophys. Res. Lett. 41 (22), 7763–7769. https://doi.org/10.1002/2014GL061541.

Rohde, R.A., Hausfather, Z., 2020. The Berkeley Earth land/ocean temperature record. Earth Syst. Sci. Data 12 (4), 3469–3479. https://doi.org/10.5194/essd-12-3469-2020.

Rohde, R., Muller, R., Jacobsen, R., Perlmutter, S., Rosenfeld, A., Wurtele, J., et al., 2013. Berkeley earth temperature averaging process. Geoinformatics & Geostatistics: An Overview 1 (2), 1–13. https://doi.org/10.4172/gigs.1000103.

Santer, B.D., Bonfils, C., Painter, J.F., Zelinka, M.D., Mears, C., Solomon, S., et al., 2014. Volcanic contribution to decadal changes in tropospheric temperature. Nat. Geosci. 7 (3), 185–189. https://doi.org/10.1038/ngeo2098.

Schurer, A., Hegerl, G., Ribes, A., Polson, D., Morice, C., Tett, S., 2018. Estimating the transient climate response from observed warming. J. Clim. 31 (20), 8645–8663. https://doi.org/10.1175/JCLI-D-17-0717.1.

Seneviratne, S.I., Zhang, X., Adnan, M., Badi, W., Dereczynski, C., Di Luca, A., Ghosh, S., Iskandar, I., Kossin, J., Lewis, S., Otto, F., Pinto, I., Satoh, M., Vicente-Serrano, S.M., Wehner, M., Zhou, B., 2021. Weather and climate extreme events in a changing climate. In: Zhai, P., Pirani, A., Connors, S.L., Péan, C., Berger, S., Caud, N., Chen, Y., Goldfarb, L., Gomis, M.I., Huang, M., Leitzell, K., Lonnoy, E., Matthews, J.B.R., Maycock, T.K., Waterfield, T., Yelekçi, O., Yu, R., Zhou, B. (Eds.), Climate Change 2021: the Physical Science Basis. Contribution of Working Group I to the Sixth Assessment Report of the Intergovernmental Panel on Climate Change [Masson-Delmotte, V. Cambridge University Press, Cambridge, United Kingdom and New York, NY, USA, pp. 1513–1766. https://doi.org/10.1017/9781009157896.013.

Seong, M.G., Min, S.K., Kim, Y.H., Zhang, X., Sun, Y., 2021. Anthropogenic greenhouse gas and aerosol contributions to extreme temperature changes during 1951–2015. J. Clim. 34 (3), 857–870. https://doi.org/10.1175/JCLI-D-19-1023.1.

Sippel, S., Meinshausen, N., Fischer, E.M., Székely, E., Knutti, R., 2020. Climate change now detectable from any single day of weather at global scale. Nat. Clim. Change 10 (1), 35–41. https://doi.org/10.1038/s41558-019-0666-7.

Slivinski, L.C., Compo, G.P., Sardeshmukh, P.D., Whitaker, J.S., McColl, C., Allan, R.J., et al., 2021. An evaluation of the performance of the twentieth century reanalysis version 3. J. Clim. 34 (4), 1417–1438.

Stott, P.A., Christidis, N., Otto, F.E., Sun, Y., Vanderlinden, J.P., van Oldenborgh, Zwiers, F.W., 2016. Attribution of extreme weather and climate-related events. Wiley Interdisciplinary Reviews: Climate Change 7 (1), 23–41. https://doi.org/10.1002/wcc.380.

Suarez-Gutierrez, L., Müller, W.A., Li, C., Marotzke, J., 2020. Dynamical and thermodynamical drivers of variability in European summer heat extremes. Clim. Dynam. 54 (9), 4351–4366. https://doi.org/10.1007/s00382-020-05233-2.

Tan, M.L., Juneng, L., Tangang, F.T., Chung, J.X., Radin Firdaus, R.B., 2021. Changes in temperature extremes and their relationship with ENSO in Malaysia from 1985 to 2018. Int. J. Climatol. 41, E2564–E2580. https://doi.org/10.1002/joc.6864.

Thompson, A., Otto, F.E., 2015. Ethical and normative implications of weather event attribution for policy discussions concerning loss and damage. Climatic Change 133 (3), 439–451. https://doi.org/10.1007/s10584-015-1433-z.

Thorarinsdottir, T.L., Sillmann, J., Haugen, M., Gissibl, N., Sandstad, M., 2020. Evaluation of CMIP5 and CMIP6 simulations of historical surface air temperature extremes using proper evaluation methods. Environ. Res. Lett. 15 (12), 124041 https://doi.org/10.1088/1748-9326/abc778.

van Oldenborgh, G.J., van der Wiel, K., Kew, S., Philip, S., Otto, F., Vautard, R., et al., 2021. Pathways and pitfalls in extreme event attribution. Climatic Change 166 (1), 1–27. https://doi.org/10.1007/s10584-021-03071-7.

Wu, Y., Miao, C., Sun, Y., AghaKouchak, A., Shen, C., Fan, X., 2021. Global Observations and CMIP6 Simulations of Compound Extremes of Monthly Temperature and Precipitation. GeoHealth, e2021GH000390. https://doi.org/10.1029/2021GH000390.

Yin, H., Sun, Y., Donat, M.G., 2019. Changes in temperature extremes on the Tibetan Plateau and their attribution. Environ. Res. Lett. 14 (12), 124015 https://doi.org/10.1088/1748-9326/ab503c.

Zelinka, M.D., Myers, T.A., McCoy, D.T., Po-Chedley, S., Caldwell, P.M., Ceppi, P., et al., 2020. Causes of higher climate sensitivity in CMIP6 models. Geophys. Res. Lett. 47 (1), e2019GL085782.

Zhang, X., Hegerl, G., Zwiers, F.W., Kenyon, J., 2005. Avoiding inhomogeneity in percentile-based indices of temperature extremes. J. Clim. 18 (11), 1641–1651. https://doi.org/10.1175/JCLI3366.1.

Zhang, J., Lindsay, R., Schweiger, A., Steele, M., 2013. The impact of an intense summer cyclone on 2012 Arctic sea ice retreat. Geophys. Res. Lett. 40 (4), 720–726. https://doi.org/10.1002/grl.50190.

Zwiers, F.W., Zhang, X., Feng, Y., 2011. Anthropogenic influence on long return period daily temperature extremes at regional scales. J. Clim. 24 (3), 881–892. https://doi.org/10.1175/2010JCLI3908.1.